European Journal of Pharmaceutics and Biopharmaceutics 151 (2020) 32–44

Contents lists available at ScienceDirect

European Journal of Pharmaceutics and Biopharmaceutics

journal homepage: www.elsevier.com/locate/ejpb

Research paper

3D characterisation of dry powder inhaler formulations: Developing X-ray micro computed tomography approaches

P. Gajjar[a,*], I.D. Styliari[b], T.T.H. Nguyen[c], J. Carr[a], X. Chen[d], J.A. Elliott[d], R.B. Hammond[c], T.L. Burnett[a], K. Roberts[c], P.J. Withers[a,e], D. Murnane[b,*]

[a] Henry Moseley X-ray Imaging Facility, Department of Materials, School of Natural Sciences, The University of Manchester, Manchester M13 9PL, UK
[b] School of Life and Medical Sciences, University of Hertfordshire, College Lane, Hatfield AL10 9AB, UK
[c] Centre for the Digital Design of Drug Products, School of Chemical and Process Engineering, University of Leeds, Woodhouse Lane, Leeds LS2 9JT, UK
[d] Department of Materials Science & Metallurgy, 27 Charles Babbage Road, Cambridge CB3 0FS, UK
[e] Henry Royce Institute for Advanced Materials, Oxford Road, Manchester M13 9PL, UK

ARTICLE INFO

Keywords:
X-ray computed tomography
Microstructural equivalence
Powder characterisation
Inhalation
Laser Diffraction
Microstructure

ABSTRACT

Carrier-based dry powder inhaler (DPI) formulations need to be accurately characterised for their particle size distributions, surface roughnesses, fines contents and flow properties. Understanding the micro-structure of the powder formulation is crucial, yet current characterisation methods give incomplete information. Commonly used techniques like laser diffraction (LD) and optical microscopy (OM) are limited due to the assumption of sphericity and can give variable results depending on particle orientation and dispersion. The aim of this work was to develop new three dimensional (3D) powder analytical techniques using X-ray computed tomography (XCT) that could be employed for non-destructive metrology of inhaled formulations. α-lactose monohydrate powders with different characteristics have been analysed, and their size and shape (sphericity/aspect ratio) distributions compared with results from LD and OM. The three techniques were shown to produce comparable size distributions, while the different shape distributions from XCT and OM highlight the difference between 2D and 3D imaging. The effect of micro-structure on flowability was also analysed through 3D measurements of void volume and tap density. This study has demonstrated for the first time that XCT provides an invaluable, non-destructive and analytical approach to obtain number- and volume-based particle size distributions of DPI formulations in 3D space, and for unique 3D characterisation of powder micro-structure.

1. Introduction

Drug delivery to the lungs is a highly desirable but extremely challenging field in pharmaceutical sciences. Pulmonary drug delivery has the advantage of allowing targeted administration directly to airways for local activity, or by delivery to the alveolar region for quick absorption into the blood stream with rapid systematic onset [24,47]. The challenge is to engineer a drug formulation that can reach the deep lungs in a portable dosage form that can be easily aerosolised and hence administered when required [8].

Dry powder inhalers (DPIs) consist of a powder mixture of active pharmaceutical ingredients (API) and inert carriers (excipients) contained in a device that deagglomerates the particles upon inhalation to deliver a dose to the lung [15]. The powder itself is central to the performance of a DPI [22], and hence the powder microstructure has a critical influence. Each of the physical particle attributes, such as size, shape, morphology and surface roughness, has an impact on the powder behaviour [34], together with the spatial organisation and correlation between the particles.

The API particles are typically produced via micronisation to reach the desirable size range of 1–5 μm required for inhalation. However, such micronised particles are not easily dispersed upon inhalation as they are highly cohesive and prone to agglomeration [13]. In order to improve the flowability and dispersibility of the formulation, the API fines are blended with larger coarse carrier particles, usually α-lactose monohydrate with particle sizes >100 μm [49,64], while intrinsic lactose fines can also be added to improve the aerosolisation performance [23,26,31]. Upon inhalation, the coarse lactose carriers are more likely to be deposited by inertial impaction in the oropharynx and upper respiratory tract, while the micronised API aerosols can achieve deep lung deposition. Aerosol deposition mechanisms have been reviewed extensively in the literature [9].

* Corresponding authors.
E-mail addresses: parmesh.gajjar@alumni.manchester.ac.uk (P. Gajjar), d.murnane@herts.ac.uk (D. Murnane).

https://doi.org/10.1016/j.ejpb.2020.02.013

Available online 05 April 2020

Table 1
Summary of different techniques currently used for understanding the structure of DPI formulations. ∗Methods which are 2D projections of 3D surfaces are classified as 2D.

Technique	Single species			Resolution	2D∗/3D	Advantages	Disadvantages
	Size	Shape	Roughness				
Laser diffraction (LD)	✓	×	×	0.5 μm	3D	Large numbers of particles can be analysed very quickly	Assumes spherical particles. Particles need to be dispersed.
Optical microscopy (OM)	✓	✓	✓	1 μm	2D	Quick and easy to use. Readily available.	2D data.
Scanning electron microscopy (SEM)	✓	✓	✓	10 nm	2D	High magnification	2D data.
X-ray computed tomography (XCT)	✓	✓	✓	2.5 μm	3D	Full 3D information on particle attributes and spatial organisation	Slow acquisition and analysis speed

DPIs are also heavily dependent on powder flow, through metering, fluidisation and dispersion. The flow of the powders is linked to the spatial organisation and correlation of the particles, which in turn is influenced by the physical attributes of the carrier [43,47,54]. For example, while a decrease in carrier size causes a decrease in the API-carrier interactions and as such an increase in drug detachment [36], the increased amounts of intrinsic carrier fines as a result of the carrier communition result in reduced flowability [53]. At the same time, increased carrier roughness can result in API fines fitting into cavities and thus not readily dispersed upon inhalation [11]. Lactose properties and their connections to DPI performance have been extensively reviewed elsewhere [34,49] and are constantly under investigation. The connection between particle properties and flow behaviour has also been recently reviewed [6,55].

The most commonly used techniques for characterising physical powder attributes are laser diffraction (LD), scanning electron microscopy (SEM), optical microscopy (OM) and cascade impaction (CI), but each have their own limitations; for example LD measurements provide the volume-based particle size distribution, but suffer from shape-bias [62] as the technique assumes spherical particles as opposed to the tomahawk shape typical of lactose crystals [51]. Microscopy-based techniques like SEM and OM are based on the 2D image analysis of particles dispersed on a substrate to produce particle size distributions and shape metrics such as aspect ratio and circularity. However, the results are highly dependent on the crystal orientation on the substrate. Another shared limitation of all these techniques is that they depend on powder dispersion and are destructive. Yet despite these limitations, LD, SEM, OM and CI have become the industrial standards for size and shape characterisation due to the lack of a suitable alternative.

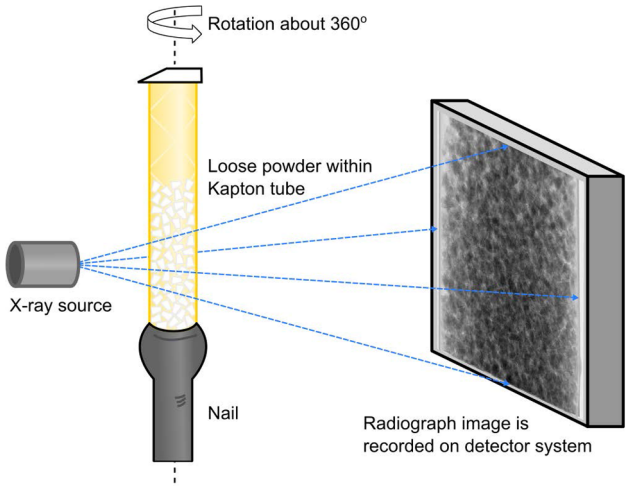

Fig. 1. The X-ray computed tomography setup involves an X-ray source producing a cone beam of X-rays that illuminates the sample. A shadow projection image (radiograph) is recorded on the detector system, and projections from different angles can be reconstructed to form a virtual volume.

Microstructure can also be assessed when studying the fluidisation and ease of dispersion of cohesive DPI powders. Particle image velocimetry (PIV) [18] and fluorescent imaging [41] employ 2D cameras to study the flow velocity and spatial distributions of API fines respectively while LD airflow titration experiments have also been employed to study the ease of de-agglomeration [5,25]. However, cohesiveness is only an indirect indicator of the microstructure. A summary of the most common characterisation techniques with their advantages and disadvantages is given in Table 1.

The most common indicator of the flowability of a powder is its compressibility, which is typically measured by comparing the bulk densities of a tapped and loosely packed powder column [65]. Other methods for measuring powder flowability include the angle of repose, or measuring the time taken to flow out of a funnel with a well-defined orifice. Although flowability is a bulk metric, it is dependent on particle level arrangements, with particle size and shape known to be influencing factors [20,65]. None of these techniques provide any insight on spatial organisation and correlation, and hence the ways in which physical attributes affect flowability at the particle level. Ring shear testers (RST) can be used to measure the flowability of a powder through a flow function coefficient (ff_c) whilst providing information on the bulk cohesion and angle of friction [32,61]. Thus RST can also provide a useful link between particle size & shape, and the powder flow properties. SEM can provide some information about the particle-particle contacts but this is limited to a 2D projection.

The sample-destructive nature of the aforementioned techniques, their shape-assumptions as well as their 2D-based description are well-known deficiencies. The need to fully characterise the microstrucure of DPI formulations has recently become more important due to the introduction of “microstructural equivalence” from the Food and Drug Administration (FDA) [35,37,50]. To this end, X-ray computed tomography (XCT) [19,39] has increasingly gained interest as a non-destructive technique to study the microstructure of pharmaceutical formulations.

XCT is well-established in the fields of material and medical sciences [38,63], and the general principles are shown in Fig. 1. An X-ray source illuminates the sample with X-rays and the transmitted X-rays are captured within the detector system. Each of these radiographs are known as single projection and, by rotating the sample through 360°, a large number of projections are acquired. All of the projections are then mathematically reconstructed using a suitable algorithm, such as the FDK algorithm by Feldkamp, Davis and Kress [14], to form a virtual volume.

The virtual volume produced through XCT is a 3D representation of the sample, allowing direct measurement of size and shapes of a particle on micron scales in complex and heterogeneous systems such as powders [52] along with 3D spatial correlation between different parts of the sample. Thanks to the above, XCT has already found applications of pharmaceutical interest. Initially such applications were focused on tablets: imaging density distributions [59], examining particle movements during compaction [16], and even hydration profiles of caffeine

and thoephylline anhydrate [46]. It has also been used to study particle coatings [48], fine granules [45], particle hollowness [28] and the microstructure of microcrystalline cellulose [12]. Recent developments in source and detector technology have improved the resolution and scanning speeds of laboratory machines [38], and coupled with falling capital costs [29], they have made XCT a more accessible laboratory technique. As a result, pharmaceutical applications have started to become more diverse with phase separation in solid dispersions [2] and drug release over time [21] being studied.

The invaluable powder microstructural descriptors that can be extracted by XCT along with the spatial relation between particles make the technique very appealing in the inhalation pharmaceutics field. As the most common excipient for inhalation formulations, characterising α-lactose monohydrate is very important. In this work, we characterise tabletting and inhalation grade lactose using XCT. Tabletting grades were studied first in order to develop the imaging conditions and image analysis workflows without the complication of small or non-uniform particle size distributions typical of inhalation grade lactose. The microstructure of individual particles within a powder bed is of importance for inhalation formulations, hence the morphology, size and shape distributions are extracted and compared with scanning electron microscopy, laser diffraction and optical microscopy to show the benefits of full 3D analysis. Proof-of-concept powder consolidation experiments were also conducted and compared with existing techniques to show the value of 3D spatial information in understanding flowability at a particle level. With the workflows established, the approach was extended from the tabletting grades to analyse the more challenging inhalation grade powders.

2. Materials and methods

2.1. Powder preparation

Two commercial tabletting-grade α-lactose monohydrate powders (CapsuLac 60 and Tablettose 70) were provided from Meggle (Molkerei MEGGLE Wasserburg GmbH & Co. KG, Germany), whilst inhalation grade α-lactose monohydrate, namely Lactohale 100 (sieved) and Lactohale 200 (milled), was provided by DFE Pharma (Goch, Germany). All powders were analysed as received.

A binary particle blend was prepared consisting of a mixture of 0.133 g Terbutaline Sulphate (TBS) and 1.2 g CapsuLac 60 (mass ratio 1:9) in a 15 ml glass vial. The blending vial was tumbled using a Turbula shaker-mixer (Willy A Bachofen AG, Basel, Switzerland) at a frequency of 30 Hz for 1 h.

2.2. Laser Diffraction (LD)

Particle size measurements were performed on a Sympatec HELOS/RODOS Laser Diffraction (LDA) unit, using the ASPIROS dispersing system with a dispersing aperture diameter of 4 mm and a feed velocity of 25 mm s^{-1} (Sympatec GmbH, Clausthal-Zellerfel, Germany). The R5 lens (measuring range 4.5 μm to 875 μm) was fitted for the measurements. Powder was filled into the ASPIROS glass vials and was dispersed via vacuum suction. Airflow titration measurements were performed following a previously established protocol [25]. The primary pressure (PP) was manually set at 0.2 bar using the adjustment valve and three measurements were taken using freshly loaded powder. Particle size distributions were calculated using Fraunhofer theory and were analysed in WINDOX 5.3.1.0 software, while further analysis was performed in MATLAB. Particle size measurements for a complete airflow titration curve were conducted on a single day.

2.3. Optical Microscopy (OM)

Optical microscopy was used to carry out particle size and shape analysis of the different powders using a Morphology G3 Particle Characterization system from Malvern Instruments Ltd. (Worcestershire, UK). A 26 mm^3 sample of each tabletting grade lactose was dispersed onto a glass plate using the systems automated sample dispersion unit at a pressure of 0.5 bar. Control of the dispersion pressure, injection time and settling time ensures high reproducibility of powder dispersion compared with a manual dispersion method. Particle imaging was performed using a × 5 magnification lens (6.5 μm to 420 μm resolution range) to ensure any larger particles or agglomerates were captured. In order to ensure an even dispersion of the inhalation grades Lactohale 100 and Lactohale 200 with minimal touching particles, smaller volumes of 11 mm^3 and 7 mm^3 were used respectively together with a dispersion pressure of 2.0 bar. The automated image analysis captures a two dimensional (2D) image of a 3D particle projected on the glass plate and calculates various size and shape parameters from the 2D image. The size and shape distributions were derived by combining the results for every particle in the sample. The particle size distribution was measured using Circle Equivalent (CE) diameter, namely the diameter of a circle with the same area as the 2D image of the particle. The number-based size distribution was converted to volume-based distribution using volumes of spheres with the measured diameters. The shape was characterised by the aspect ratio and circularity. The aspect ratio is given by the ratio of the shortest distance to the longest distance in the image of the particle, whilst circularity (Eq. (1)) is the 2D equivalent of the sphericity (Eq. (2)) and is given by the weighted ratio of the particle area A to the perimeter P:

$$\text{circularity} = \frac{\sqrt{4\pi A}}{P}. \quad (1)$$

2.4. Scanning Electron Microscopy (SEM)

The powders were deposited onto adhesive carbon tabs (Agar Scientific G3357N), which were pre-mounted onto aluminium stubs (Agar Scientific JEOL stubs G306) and then sputter-coated with gold for 1 min to achieve a thickness of around 30 nm (Quorum SC7620) in order to reduce electrostatic charging. The images were acquired using a JEOL 5700 scanning electron microscope, operated at 20 kV and a working distance of 10 mm.

2.5. X-ray computed tomography (XCT)

A sample mount for XCT was created by gluing 3 mm diameter Kapton (polyamide) tubing of length 25 mm onto a nail. Each powder plug was prepared by filling a separate sample mount with powder using a spatula, before gluing a small piece of paper on the top to seal the tube. Scans were performed at the Henry Moseley X-ray Imaging Facility using a Zeiss Xradia Versa 520 cabinet X-ray microtomography system, with the acquisition parameters given in Table 2. The Versa family of instruments are particularly suited to scanning low density powders, as the detector system uses X-ray optical lenses for magnification, allowing small working distances that minimise the absorption loss in air. In addition, the coherent source within the Versa family allows in-line X-ray phase contrast that is useful in the segmentation [40]. Virtual volumes for each sample were computationally reconstructed from the projection images using the native Zeiss reconstruction software. The voxel size of the reconstructed volume is equal to the acquisition pixel size cubed, with the minimum resolvable feature being ~3 × the voxel size.

A single slice through a virtual volume of a CasuLac 60 powder bed is shown in Fig. 2A. There are distinct greyscale values for two phases present, with the denser lactose having brighter pixels and the less dense air having darker pixels. The coherence of the source, small working distances and low density material all combine to produce in-line phase contrast, with identifiable phase fringes at the edges of the particles. A zoomed-in section of the same slice is provided in Fig. 2B,

Table 2
XCT scanning parameters used on a Zeiss Xradia Versa 520 microtomography system for the different sample types.

Sample	Voltage (kV)	Power (W)	Exposure (s)	Projections	Binning Mode	Objective Lens	Source distance (mm)	Detector distance (mm)	Pixel Size (μm)
CapsuLac 60, Tablettose 70 (Characterisation)	80	7	3.5	3201	1×	4×	12	14	1.56
CapsuLac 60, Tablettose 70 (Tap Density)	120	10	0.8	1601	2×	4×	27	19	4.00
Lactohale 100, Lactohale 200	80	7	3.5	3201	1×	10×	12	14	0.64
Terbutaline sulfate (10% w/w) Blend	40	3	12.5	1601	2×	10×	12	14	1.27

which shows a very bright ring around the inside boundary edge of the particle and a dark ring around the outside boundary edge.

The data was filtered using an edge-preserving filter such as a bilateral filter or a 2D non-local means, and the lactose separated from the air using a global automatic greyscale thresholding as shown in Fig. 2C. In order to separate the individual grains, a binary image was produced of the particle edges, with the phase fringes producing a sharp morphological image gradient. Morphologically combining the phase fringes with the lactose mask created marker labels for each particle, which were expanded out to each fill each particle using a watershed algorithm [68]. This produced a labelled image in which all of the voxels of an individual particle are assigned the same integer value, as can be seen in Fig. 2D.

This approach for creating marker labels is different from the common approach of using distance maps [69], where each pixel within the particle is assigned a value according to its euclidean distance from the edge of the particle. The distance map method works well for spherical grains since the centre of a sphere is a local maximum of the distance from the edge of the grains. However, for the non-spherical lactose grains, the distance map could be seen through visual inspection to consistently over-segment particles [3], i.e. excessively separating particles so that they were too small. Instead the X-ray phase contrast

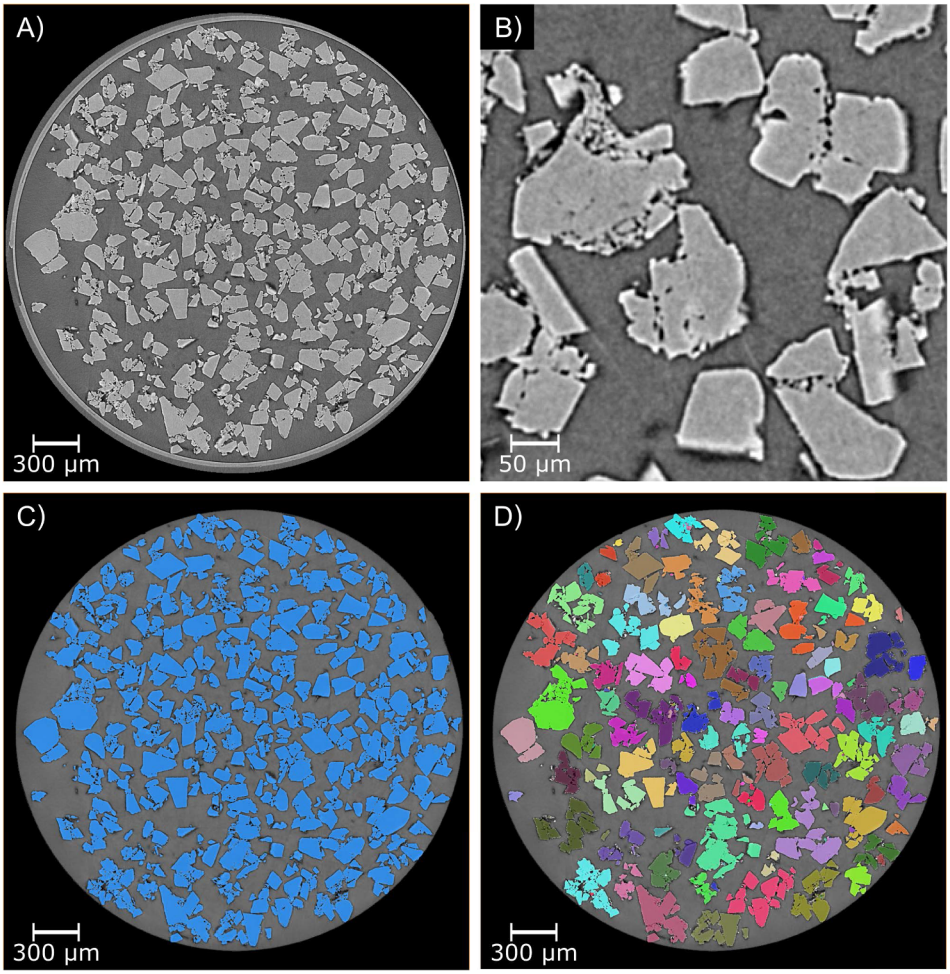

Fig. 2. (A) A single horizontal slice through the virtual tomographic volume of CapsuLac 60. (B) α-lactose monohydrate exhibits phase contrast when scanned, with a bright ring inside the particle boundary edge and a dark ring outside the boundary; (C) Lactose segmented from air; (D) All particles separated and shown with a different colour per particle, with this slice containing 176 unique particles.

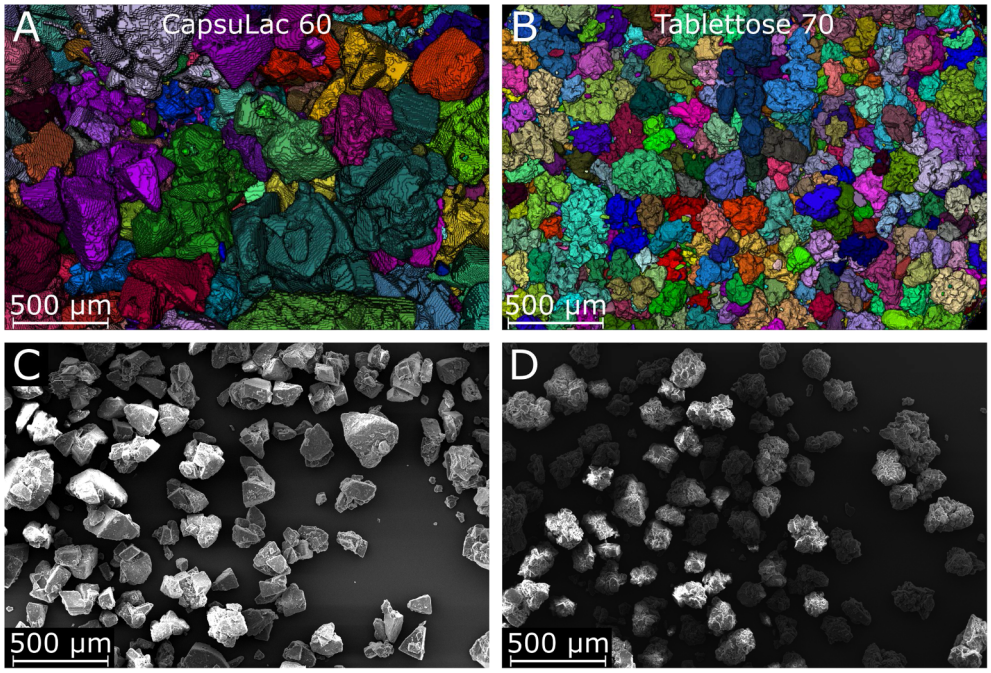

Fig. 3. Morphology of the tabletting lactose grades produced through XCT (A & B) and SEM (C & D). The XCT images are coloured with a different colour for each separated particle. (For interpretation of the references to colour in this figure legend, the reader is referred to the web version of this article.)

fringes provide contrast between lactose and air, and were exploited to provide confident differentiation between particles that are more than one pixel-width apart (Table 2). For reference, the pixel-size for scans of tabletting grades and inhalation grades was 1.56 μm and 0.64 μm respectively. Visual inspection showed that the phase contrast approach provided a better segmentation than the distance map approach, without under- or over-segmenting the grains.

The labelled image can be processed to produce volume, size and shape measurements for each particle. The volume of a particle is simply the summation of all voxels assigned to that particle, which can also be used to give the particle size as the diameter of a sphere with an equivalent volume. The three-dimensional representation gives three distinct lengths, namely eigenvalues of the moments of inertia matrix of the particle known as length, breadth and width in decreasing order of magnitude. Taking pairs of these gives three aspect ratios [58]. The sphericity is a measure of how spherical a particle is, and is defined as the ratio of the surface area of an equivalent volume sphere S_{eq} to the actual 3D surface area of the particle S, i.e.

$$\text{sphericity} = \frac{S_{eq}}{S} = \frac{\pi^{1/3}(6V)^{2/3}}{S}, \tag{2}$$

where V is the actual particle volume.

2.6. Powder densification and consolidation

Powder densification studies were performed using XCT and a Copley Tap Density instrument. The tap density measurements on the Copley instrument were performed by pouring 10 g of powder into a 25 ml volumetric cylinder and noting the volume before and after 1000 taps. The measurements were performed in triplicate and the experimental error was ± 0.25 ml. The XCT densification was measured through a series of scans using larger 14 mm diameter Kapton tube to prevent fluidisation, with a 4 mm cubic region of interest at the bottom of the tube. The tube was filled with powder using a funnel up to a height of 42 mm (approx. 6.5 ml) and the first scan performed. The entire sample holder was then tapped by hand 500 times and a second scan performed. Different scanning parameters were used due to the larger amount of material for the X-rays to pass through, which are given in Table 2. In order to calculate the density from the virtual volumes, the first 40 slices were removed from the top and bottom of the final volumes due to cone beam artefacts. As in Section 2.5, the virtual volumes were filtered and global thresholding used to identify lactose voxels. The total number of lactose voxels was sufficient for the tap density, as the number is directly proportional to the volume of lactose within the imaged volume that is constant for both scans. The amount of lactose can be expressed as a volume fraction (VF), from which Carr's index can be calculated as:

$$\text{Carr's index} = 100 \times \left(1 - \frac{\text{VF}_{\text{pre-tap}}}{\text{VF}_{\text{post-tap}}}\right). \tag{3}$$

An alternative measure of flowability is the Hausner Ratio, which can be calculated as:

$$\text{Hausner ratio} = \text{VF}_{\text{post-tap}}/\text{VF}_{\text{pre-tap}}. \tag{4}$$

2.7. Ring shear testing (RST)

The ring shear testing technique was applied for the evaluation of the flow properties of the powder samples. Each measurement was performed using the ring shear tester, RST-XS (Dietmar Schulze, Germany). At the beginning of the measurement, the powder sample was filled into a 30 ml annular shear cell without applying force to the upper surface of the powder bed. The powder was then consolidated under a pre-shear normal consolidation stress of 2 kPa and the lower portion of the cell was slowly rotated until a steady state flow had been achieved. After the pre-shear process, the normal stress was first released and a lower normal stress was then applied to shear the powder until the incipient flow occurred in the powder sample. The incipient shear stresses were measured at three different normal stresses (0.4, 1.0 and 1.6 kPa). A yield locus was constructed for each powder and the respective flowability index (ff_c) was calculated using the instrument software. The results were repeated for pre-consolidation stresses of 5 kPa and 10 kPa.

3. Results

3.1. Tabletting grades

3.1.1. Particle morphology

The final segmented volume, containing virtual representations of every particle, provides a wealth of 3D information. Three-dimensional visualisations allow the complete particle morphology to be assessed, as shown in Figs. 3A and B with each separated particle represented by a unique colour. SEM is a commonly used technique for assessing morphology, and SEM images of a corresponding scale are shown below in Fig. 3C and D. CapsuLac 60 is a sieved grade that is known to contain individual single crystals, with some agglomerates. This can be seen in the XCT morphology in Fig. 3A with many crystals showing typical lactose "tomahawk" shapes with clear facets. On the other hand, Fig. 3B shows Tablettose 70 to have a more rounded structure, which is consistent with the manufacture of the powder through continuous spray dry agglomeration. The XCT shows more agglomeration than the SEM images. This is likely due to the dispersion needed to prepare the suspension on the SEM slide, which would break up weakly connected particles. The 3D void space (ϕ) between particles can be further quantified by XCT with results given in Table 3.

3.1.2. Particle size distribution

Beyond simple visualisation, the virtual particle representations can be used to quantify the particle size and shape. By summing the voxels of that particle, XCT calculates its actual volume without any *a priori* assumptions. This is in contrast to LD, which assumes that particles are spherical with a specified adjustment factor, and to OM/SEM, which calculates the volume of a sphere with an equivalent diameter to that of the projected area. Note that OM is more routinely used for size analysis than SEM due to the lower magnification, lack of coating and automated workflows of machines such as Morphologi G3 (Malvern, UK). The number of unique particles within the sampled volume for XCT was 5120 and 12976 for CapsuLac 60 and Tablettose 70 respectively, whilst the corresponding number of sampled particles for OM were 4609 and 11262. A comparison of the particle size-distributions produced by the LD, XCT and OM is shown in Fig. 4, with a non-logarithmic x-axis used to highlight differences in the distributions. The shape of the distributions are broadly similar across the methods, which provides confidence that the segmentation method is neither systematically under-segmenting nor over-segmenting the particles. Whilst visual inspection shows locally on single cross-sectional slices whether the image analysis method is under-segmenting or over-segmenting, the size-distribution gives a meso-scale reference over all of the particles. In the case of under-segmentation, the XCT curve would be shifted significantly to the right compared to LD and OM, whilst case of over-segmentation the XCT curve would be shifted significantly to the left. However it is found that the XCT curves show good overlap with the other methods for all of the powders examined thus validating the quality of segmentation.

Looking more closely, the XCT distribution is narrower and has a slightly lower modal value for both powders compared to LD and OM. This can also be appreciated by examining the 10th (D10), 50th (D50) and 90th (D90) percentiles of particle size in Table 4. The lower modal and percentile values for XCT are due to it measuring the actual volume of the particle. On the other hand, the assumption of particle sphericity used in both LD and OM means that the reported sizes are overestimates of the actual particle sizes [62]. This is the main reason that the XCT distributions lie to the left of LD and OM, rather than being due to the resolution limits of either technique. It is also noteworthy that whilst the XCT and LD statistics are broadly comparable, those of OM are of the order of 20 μm larger. This is because the size distribution is based on a single 2D projection of the particles, and can vary significantly depending on the direction imaged. This also has a significant impact on the particle shape analysis. The XCT size distributions show a significant right-hand tail, which is likely to be due to the presence of aggregates that would not be separated as there is no dispersion in the powder preparation.

Table 3
3D measurements of the void fraction ϕ (defined as the ratio of void volume to total analysis volume) from XCT, for each of the tabletting and inhalation lactose grades. Lactohale 100 and Lactohale 200 abbreviated as LH100 and LH200 respectively.

CapsuLac 60	Tablettose 70	LH100	LH200
0.562	0.548	0.402	0.409

3.1.3. Particle shape distributions

A comparison of aspect ratio and sphericity distributions for both tabletting grade powders can be found in Fig. 5. The length to breadth and breadth to width ratios broadly coincide, whilst the length to width ratio is much lower reflecting the classical tomohawk shape of lactose. This information cannot be found in the aspect ratio distribution produced by static imaging, where the 2D projections permit only two independent lengths, and hence one aspect ratio to be determined which coincides with both length-to-breadth and breadth-to-width ratios.

The sphericity/circularity distributions in Fig. 5 show a much more distinct difference between OM and XCT, which can be attributed to the difference between 2D and 3D imaging. Fig. 5B shows the sphericity/circularity for CapsuLac 60, with OM giving a broad distribution that is nearly uniform between 0.6 and 0.9. An explanation for this could be due to differences in imaging a particle from different orientations. Consider the single particle in Fig. 6, shown in two different orientations with the corresponding 2D projection underneath. The orientation in Fig. 6a has a circularity of 0.67, whilst the orientation in Fig. 6b has a circularity of 0.89. DEM simulations of different particle settling under gravity (supplementary video V1) showed that the 2D circularity can be ± 8% compared to the 3D value [7]. Thus, as the 2D circularity can vary by 15% for each particle, imaging over 5000 particles can yield a broad distribution. By contrast, the XCT displays a thin normal-like distribution with a mode of approximately 0.8, as each particle only has a single sphericity. For example the particle shown in Fig. 6 has a sphericity of 0.79. The sphericity of the tomahawk shape predicted by synthon-based modelling is 0.87 [44].

There is a clear lower tail to the XCT distribution of CapsuLac 60 in Fig. 5B, with a small number of particles having sphericities between 0.3 and 0.6. The lower sphericity is a result of the agglomerated structure. Tablettose 70 is known to have a high proportion of agglomerates, and this can be seen in its sphericity distribution in Fig. 5D with a smaller lower peak around 0.5. Although OM also gives a bimodal distribution, the lower peak is around 0.65 and is a high proportion compared to XCT.

3.1.4. Powder density and flowability

One further property that is important for inhalable powders is their flowability, which can be quantified using the Carr's index or Hausner ratio. A comparison between XCT and a benchmark of a Copley tap density instrument can be found in Table 5. Both techniques show similar results, with CapsuLac 60 showing both a slightly lower Carr's index and slightly lower Hausner ratio than Tablettlose 70, implying marginally better flowability that Tablettose 70. This can be linked back to the size and shape distributions in Figs. 4 and 5 with both powders having similar modal sphericities, but CapsuLac 60 having a larger particle size and hence lower granular Bond number [6]. Quantatively, the Carr's index and Hausner ratio calculated from XCT are larger than those of the Copley tap density instrument. As this was a proof of concept experiment to study the process of powder densification of relevance to powder flow, it should be noted there were a number of experimental factors that would contribute to the differences: 1) the initial poured state was less for XCT than for the Copley

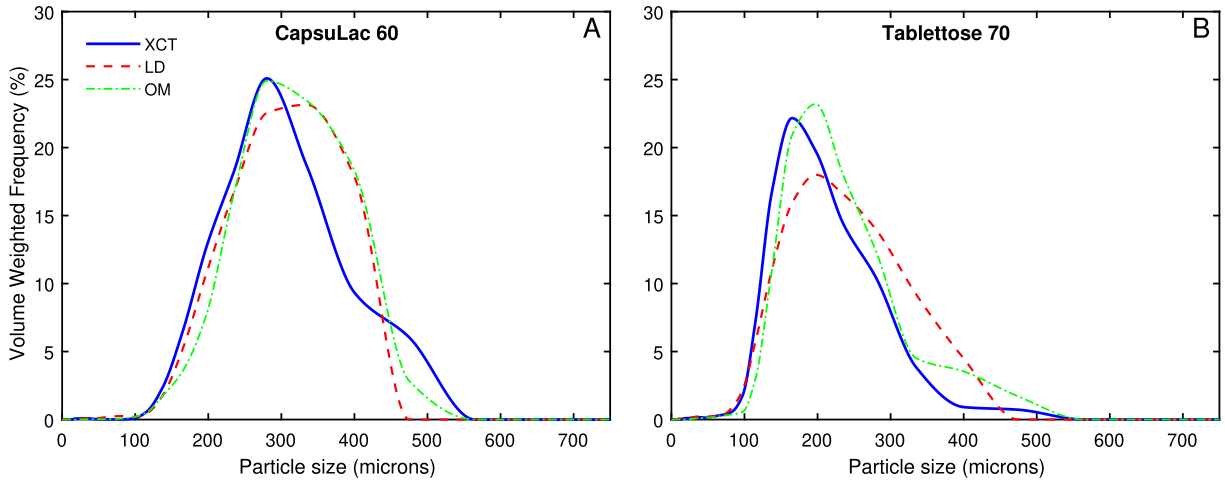

Fig. 4. Comparisons of the size distributions for the two tabletting grades produced using the X-ray computed tomography (XCT), laser diffraction (LD) and optical microscopy (OM).

Table 4
Size distributions statistics (defined in text) for tabletting grade and inhalation grade lactose produced from X-ray computed tomography (XCT), laser diffraction (LD) and optical microscopy (OM). All measurements are given in microns. †The inhalation grades were dispersed at 2.0 bar for the OM measurements.

	D10	D50	D90	D10	D50	D90
		CapsuLac 60			**Tablettose 70**	
XCT	165	251	367	113	165	256
LD	169	262	357	113	187	298
OM	183	270	367	128	183	278
		Lactohale 100			**Lactohale 200**	
XCT	49	93	121	19	67	109
LD	55	124	205	11	67	128
OM†	58	152	242	25	92	149

instrument; this would affect the final tapped state and hence Carr's index and Hausner ratio; 2) The volume of powder examined in XCT was less than with the Copley instrument; 3) The smaller diameter tube used in XCT compared to Copley means that wall effects may have more influence. As there are multiple contributing factors, a direct comparison with the Copley instrument was not appropriate, although it was possible to conclude that powder densification could be studied by XCT, analogous to the tap densitometry, albeit requiring substantially lower material sample mass.

The RST results in Fig. 7A are consistent with the tap density results in showing that both CapsuLac 60 and Tablettose 70 are free-flowing. In general, the greater the ff_c value, the more free-flowing the powder is, with powders having $ff_c > 10$ considered to be free flowing. Furthermore, CapsuLac 60 is more free flowing at low pre-consolidation stresses, but Tablettose 70 is marginally more flowable at high pre-consolidation stresses. This can be linked to the particle size and shape analysis of the two powders in Sections 3.1.2 and 3.1.3 through the bulk cohesion and angle of friction shown in Fig. 7B. CapsuLac 60 has a lower bulk cohesion, which can be explained through its larger particle size [56]. The friction angle for CapsuLac 60 decreases with pre-consolidation stress, whereas for Tablettose 70, it initially increases. This could be related to the non-spherical aggregates in Tablettose 70 that have a lower sphericity, and could prevent flow through interlocking [1].

One clear advantage of XCT is that it allows the densification and flowability to be examined in 3D, with the ability to see changes in void spaces and particle orientations. Fig. 8 shows a vertical cross-sectional slice taken at the same location of the Kapton tubing containing CapsuLac 60 and Tablettose 70 before and after tapping. The pre-tap state of both powders shows many large air pockets between particles, and although the post-tap states shows smaller void spaces between the particles, there are still a small number of larger void spaces. This would suggest that further densification is possible with more tapping, which is consistent with the lower final tapped density in XCT as compared to the Copley instrument. Qualitatively, Tablettose 70 appears to have fewer of these large air pockets in the tapped state, suggesting that it is closer to its final steady state. It would also be possible to examine spatial changes in size distribution during the densification process, but this lies outside the scope of these proof of concept studies.

3.2. Inhalation grade lactose

Inhalation grade lactose presents a bigger challenge due to its higher complexity and smaller particle sizes, however the same method can be applied. Visualisations of Lactohale 100 and Lactohale 200 can be seen in Fig. 9A and B respectively. Visual inspection shows the difference between the sieving and milling processes, with Lactohale 200 showing a higher number of intrinsic lactose fines than Lactohale 100. The number of fines can be quantified in the size distribution shown in Fig. 9C. As the maximum standard deviation between the 3 LD repeats across all sampling points was less than 0.75%, error bars were of the same order of magnitude as the line width and hence are omitted from Fig. 9C to allow a clearer comparison between XCT and LD. The number of analysed particles for XCT was 4894 and 30855 for LH100 and LH200 respectively. Both Lactohale 100 and Lactohale 200 have main peaks around 100 μm corresponding to the coarse lactose, with Lactohale 200 showing a second smaller peak around 20 μm corresponding to lactose fines. The number density of lactose fines can also be quantified through XCT by splitting the analysis region into 8 smaller cubes of side length 300 μm and counting the number of lactose fines in each cube. This gave mean densities of lactose fines as 9426 ± 559 particles per mm^3 and 66458 ± 6033 particles per mm^3 for Lactohale 100 and Lactohale 200 respectively. It is also important to know the spatial position of fines within the entire powder bulk, and this is visualised in Fig. 9D with lactose fines less than 12 μm shown in yellow and those greater than 12 μm shown in grey. A video of the positions of lactose fines in Lactohale 200 can be found in Supplementary Video V2.

Dry powder inhaler formulations also contain fine API particles together with the excipient lactose, and Fig. 10 shows a cross section through the virtual volume and a 3D visualisation of an XCT scan of a representative blend of CapsuLac 60 and TBS. Despite CapsuLac 60 being a larger and more simple powder compared to the Lactohale

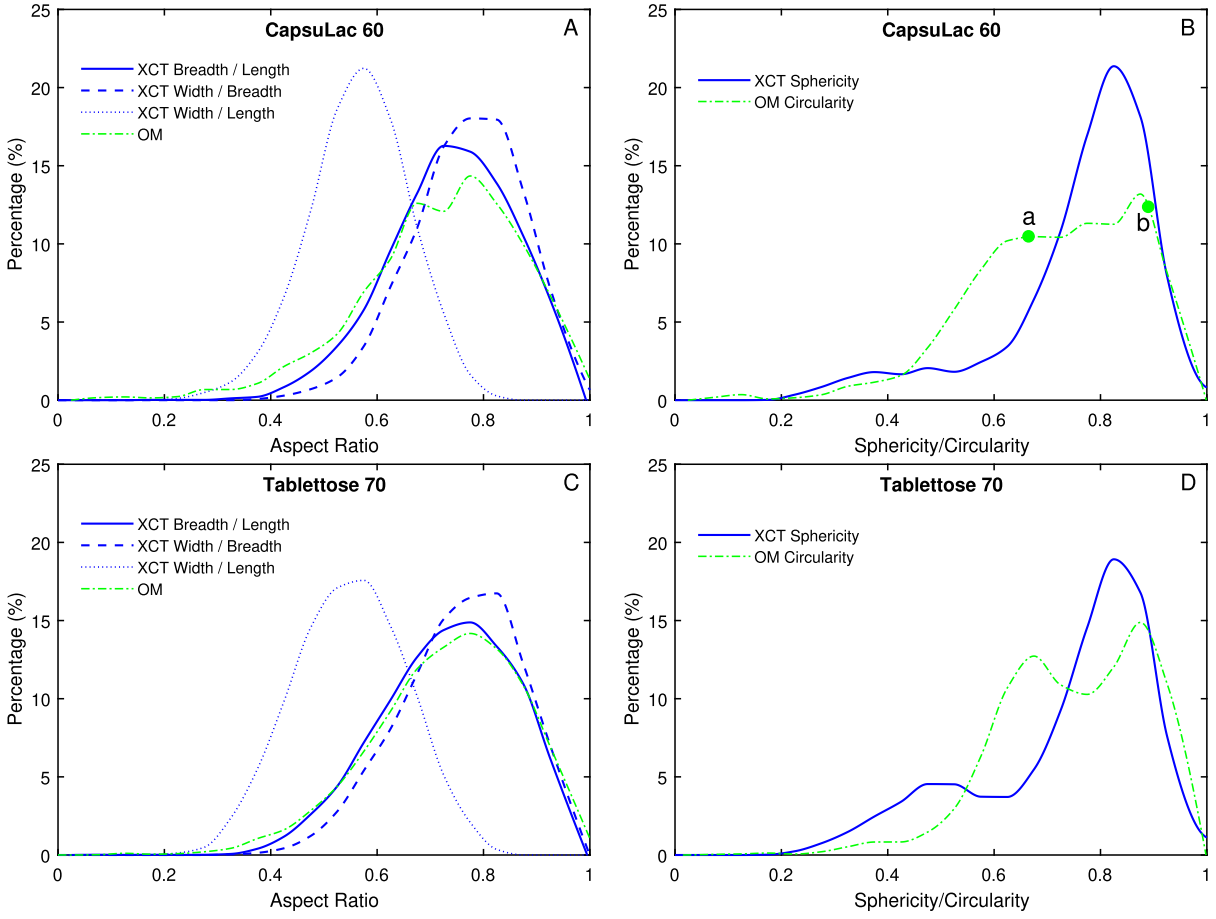

Fig. 5. Comparison of the aspect ratios and sphericity distributions for the two tabletting grades using the X-ray computed tomography (XCT) and optical microscopy (OM). Points *a* and *b* in B correspond to the 2D circularity results of a single particle projected in two different orientations, as shown in Fig. 6a,b respectively.

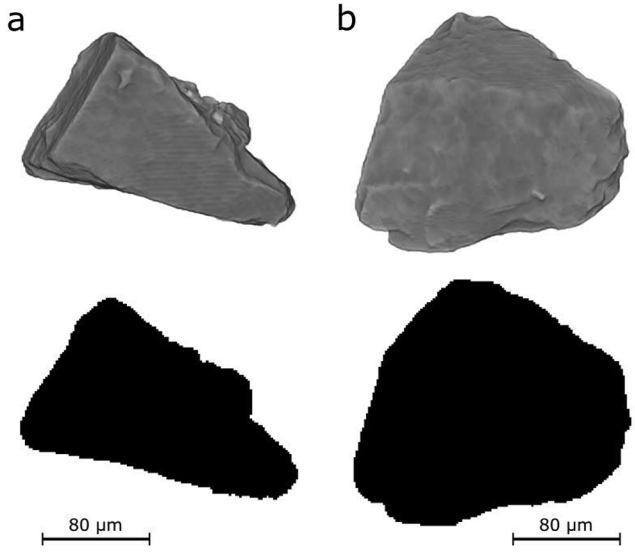

Fig. 6. Imaging a single particle from two different orientations, *a* and *b* can give circularity values of 0.67 and 0.89 respectively. For comparison, the 3D sphericity value calculated from XCT for this particle is 0.79.

grades, the representative blend highlights the complex nature of inhalation blends. Although CapsuLac 60 and TBS have differences in particle size and small differences in atomic density, Fig. 10A shows how there is very little discernible difference between the grayscale values of the two species. As a result, it is not currently possible to segment the two phases with confidence using absorption contrast and Fig. 10 does not make any attempt to differentiate between the species. Further work is currently under way to utilise phase contrast (Fig. 2B, Mayo et al. [40]) to distinguish between the different species.

Table 5
Comparison of tap density results between XCT and a Copley tap density system.

		CapsuLac 60	Tablettose 70
CT	Poured Density (g ml^{-1})	0.47	0.46
	Tapped Density (g ml^{-1})	0.54	0.53
	Carr's index	13.1	14.3
	Hausner ratio	1.15	1.17
Copley	Poured Density (g ml^{-1})	0.61	0.53
	Tapped Density (g ml^{-1})	0.66	0.59
	Carr's index	6.5	10.2
	Hausner ratio	1.08	1.11

4. Discussion

X-ray computed tomography has been widely used for characterising particulate materials, ranging from large rocks in the mining industry [42] to additive manufacturing powders [60], however the challenge in using XCT for DPI formulations is the small particle size and low atomic density. In this paper, we have shown how XCT can provide invaluable three-dimensional insight into the structure of pharmaceutical powders. In particular, the particle morphology, bulk powder void fraction, particle size and shape distributions, and tap

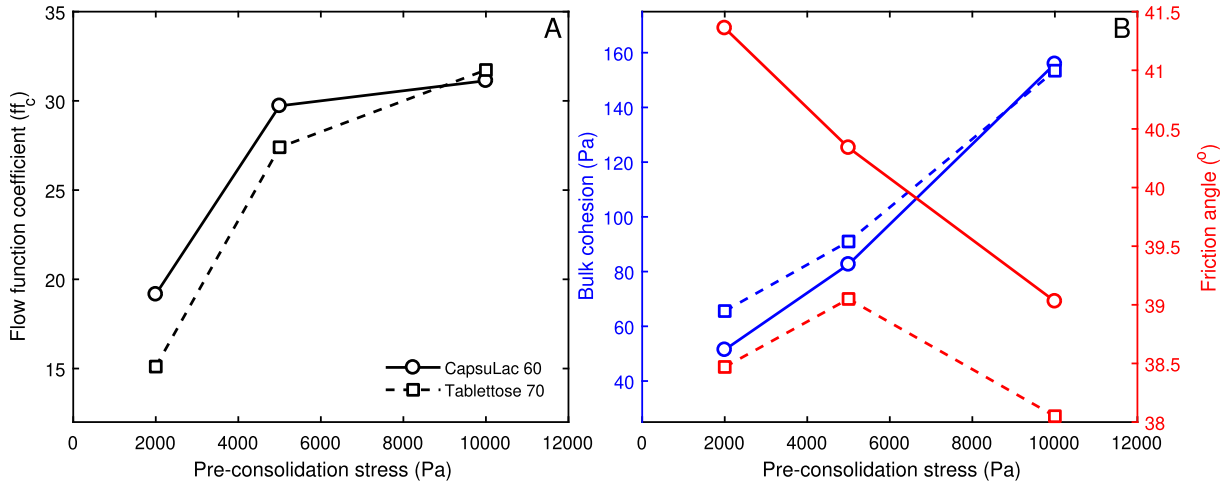

Fig. 7. (A) Flow function coefficients (ff$_c$) for CapsuLac 60 (solid line and circular markers) and Tablettose 70 (dashed line and square markers). (B) Bulk cohesion and angle of friction for the two powders using the same respective linestyles.

density measurements were collected for a tabletting grade lactose, with inhalation grade lactoses and a blend also analysed.

The particle morphology could be judged from a 3D rendering of the segmented data, and compared to SEM images of the same magnification. Although SEM images allow higher magnification from a single projection angle, the advantage of XCT is that it allows the powder to be examined from any desired angle with the minimum of sample preparation, i.e. without dispersion and with no gold coating. Correlative techniques for combining the 3D results of XCT with the magnification of electron microscopy results have been developed for metallic coatings [4], but an extension to free powder beds requires the development of a resin for fixing the bulk powder without altering the surface or internal structure.

Volumetric void fractions were easily calculated for each of the powder grades, and furthermore the void spaces can also be easily visualised. This could provide a useful connection between fluidization

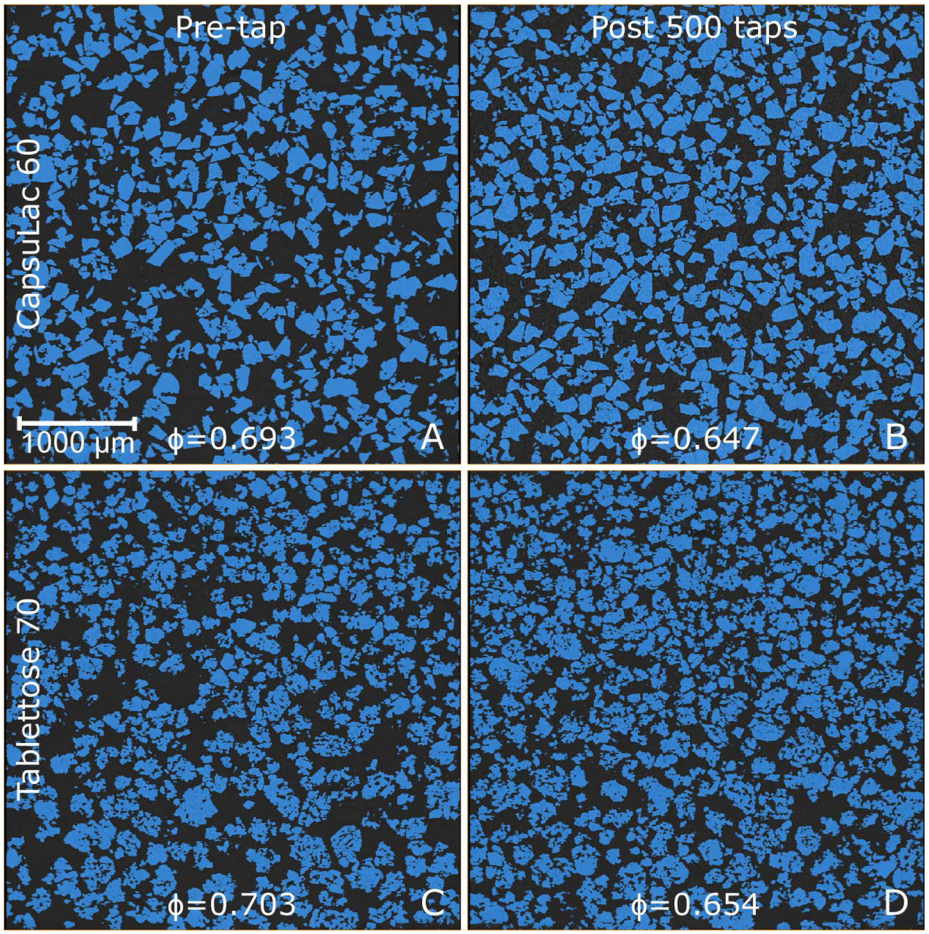

Fig. 8. Vertical cross sectional slices from virtual XCT volumes of CapsuLac 60 (A,B) and Tablettose 70 (C,D) showing the initial particle density (A,C) and the densified state following 500 taps (B,D). The lactose particles are highlighted in red and the scalebar in A is applicable to all images. Gravity is downwards.

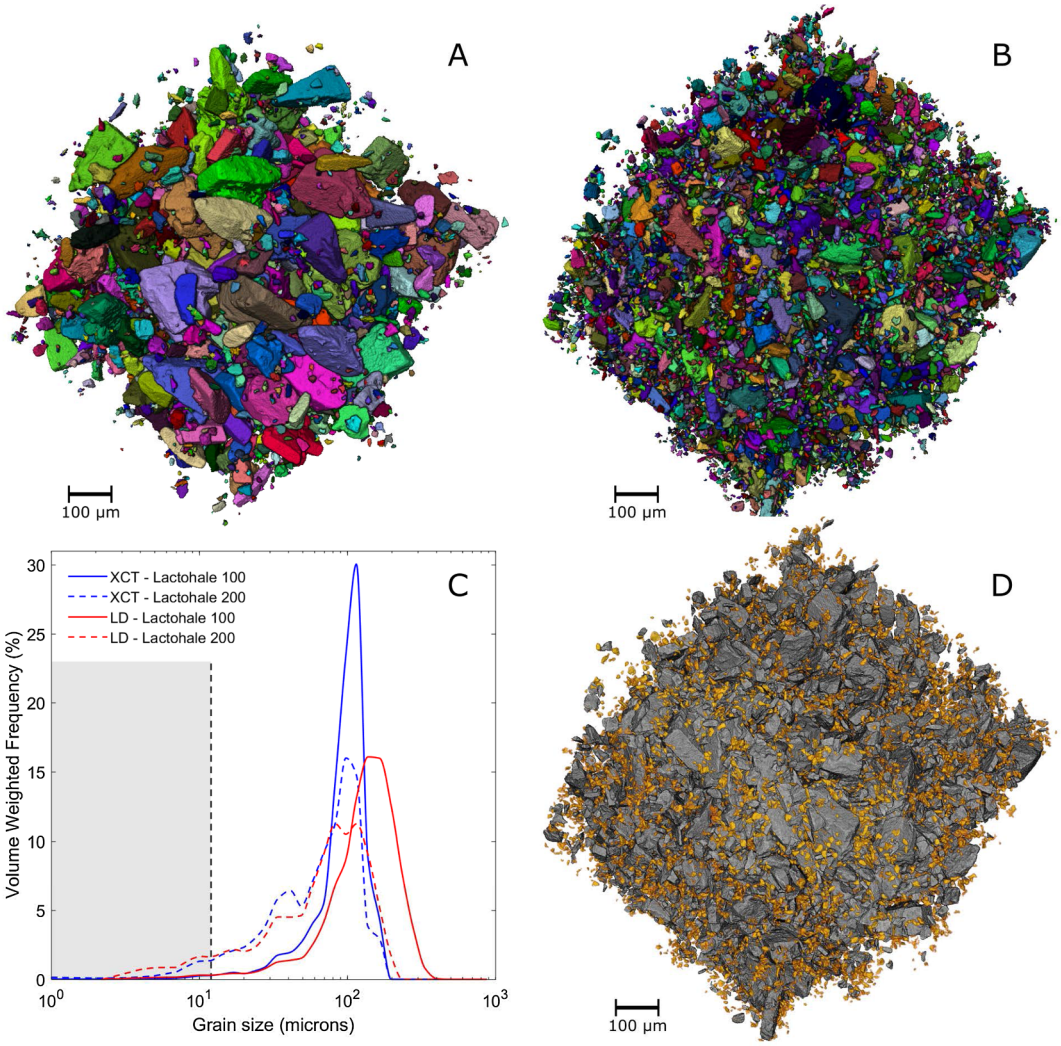

Fig. 9. 3D renderings of two inhalation grades show the difference between sieving (Lactohale 100 shown in A) and milling (Lactohale 200 shown in B) processes, with one colour per particle. Size distributions for the two grades from XCT and LD are shown in C, with fine lactose of size <12 µm highlighted in grey. The visualisation in D is the same data and orientation as B but shows the relative positions of the fine lactose (<12 µm) in orange and coarser lactose (>12 µm) shown in grey. A video of D can be seen in supplementary material video V2.

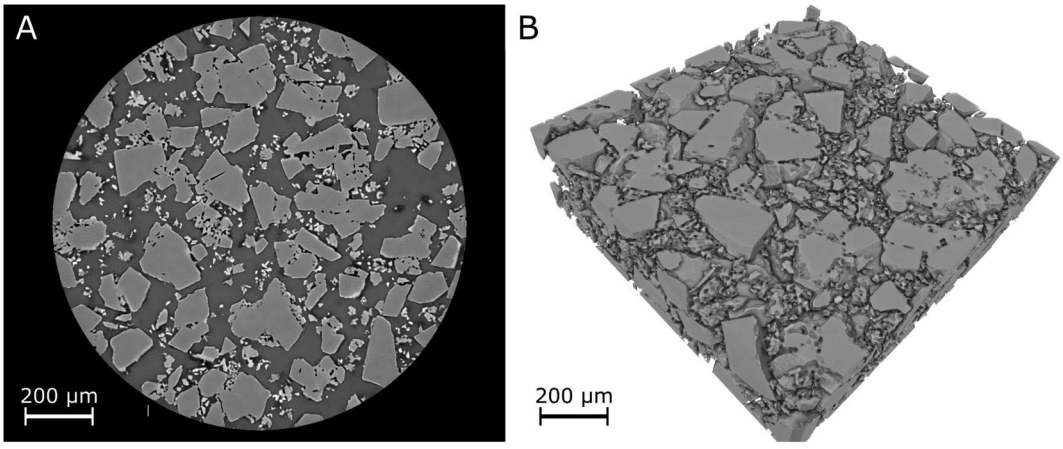

Fig. 10. A horizontal cross sectional slice (A) and 3D rendering (B) of a representative blend of CapsuLac 60 and Terbutaline Sulphate highlighting the complexity of inhalation formulations.

and aerosolization simulations [33] and experiments [66], for instance by scanning the experiment to determine the exact initial particle matrix as the starting conditions for simulations. The combination of XCT and simulations would also open new avenues for understanding the behaviour of DPI powder blends, for instance how the initial particle orientation and packing affect the aerosolisation behaviour.

It was seen that XCT produces size distributions comparable to laser diffraction and static imaging; the slightly lower sizes are a result of using all of the volumetric information of the particle with no prior assumptions. Even if XCT results are taken to be a more accurate determination of size, laser diffraction is still a more widely available industrial technique and a very fast method for size analysis. The comparable distributions give confidence that laser diffractions remains a good choice for size analysis, but work is underway to further improve LD distributions by feeding shape information from XCT into the LD non-sphericity adjustment factor.

Although size distributions were comparable between XCT and the other methods, the shape distributions produced from the 3D XCT data provided more accurate measures of the aspect ratio and sphericity than 2D static imaging. Indeed, the pitfalls of basing shape distributions from single 2D projections of particles are clearly shown with projections of a single particle. For this reason, XCT presents a clear alternative for accurate shape analysis. It should also be noted that shape and size analysis are performed in tandem on the same bulk powder, allowing cross correlations to be accurately determined. Further work is underway looking to advance the shape analysis by deriving shape factors correlated to predicted crystal geometry, along with determining how the shape affects the surface properties and binding to micro-lactose and API particles.

When comparing LD, OM and XCT, it is worth considering the different availabilities and scan times. Both LD and OM instruments are commonly found throughout both industrial and academic laboratories and allow analysis of multiple samples within several hours. Most LD and OM systems have automated work flows that require only basic user training. On the other hand, XCT systems with the highest resolution of $<1\ \mu m$ needed for examining inhalation powders have much more limited availability, and can take approximately 4-5 h to scan each sample. Furthermore, XCT systems currently require technicians experienced in both instrument operation and image processing in order to extract quantitative powder information. Relatively speaking, there is still a large capital and knowledge barrier to pharmaceutical industry use of XCT, as compared to LD and OM. Initiatives in the UK such as establishment of the Future Continuous Manufacturing and Advanced Crystallisation Research Hub[1] and the Henry Royce Institute for Advanced Materials[2] are helping to bridge the gap between universities and industry by making cutting edge material science instruments and expertise accessible to those outside academia [30].

The effect that powder microstructure has on performance is also important, and one aspect of inhalation powder performance is flowability. Particle size and shape affect the flowability, in turn affecting the emission and drug loss [27]. Flowability is intrinsically linked to particle organisation, and the proof of concept tap density studies show the potential of XCT for 3D analysis of flowability. A simple compressibility index such as Carr's index or Hausner ratio gives no insight on particle organisation, and although flow function coefficient curves provide a relation between particle size, shape and flowability, they too do not allow the flow behaviour to be visualised at the particle level. The proof of concept experiments demonstrate how XCT allows such visualisation, also providing information on particle interconnectivity, and whether particle orientations also change during tapping [67]. Scans would need to be optimised for image resolution rather than speed, and a more systematic tapping or flowing mechanism synchronised with the XCT machine would allow motion between taps to be resolved [17]. A systematic tapping mechanism would also allow a more equivalent comparison to standard tap density instruments.

XCT was also shown to be valuable analytical technique for smaller sized and more complex inhalation powders, distinguishing clear morphological differences between sieved Lactohale 100 and milled Lactohale 200. As with tabletting grades, XCT could also produce particle size distributions of the inhalation grades that are comparable to LD. In addition XCT could produce number densities of lactose fines, and also highlight their spatial positions in 3D, which is not available through any other technique. Work is currently under way to utilise this strength of XCT to examine the effects of manufacturing processes on the number and position lactose fines, and in addition, to extend the method to work with blends of carrier lactose and fine API particles.

The performance of an inhaler is fundamentally dependant on the aerodynamic behaviour of the particles, which is linked to the particle size, shape and interfacial interactions. Yet there is currently only a limited understanding of the relationships between material properties, microstructure, particle size, and powder performance [57]. In providing a direct link between size, shape, and performance attributes such as flowability, XCT has the potential to give real insight into the aerosolisation process that generates the potentially-inhalable aerosol cloud. Aerosol formation from a DPI is governed by the interaction between the inhalation airflow and a powder bed that possess a mechanical resistance to aerosolisation due to its microstructure. XCT provides the ability to study an inhalation powder's microstructure, and to begin to de-construct the aerosolisation process. Building on the simple DEM gravity settling experiments in this manuscript, more advanced DEM simulations are currently under way that utilise real 3D shapes to predict the behaviour of a bulk powder through a device and into an inhaled air stream.

Alongside the benefits of full 3D analysis, the non destructive nature of XCT makes it an important tool for examining new and potentially expensive formulations. No new DPIs have entered the market in the past 20 years, with one of the aims of future DPIs being low cost [10]. In this regard, the ability of XCT to measure size and shape from only a small amount of material and simple sample preparation whilst allowing that material to be reused in other tests should help improve development processes and efficiency. XCT offers benefits for early drug development phases, when API is typically in scarce supply, and could facilitate rapid decision-making early in development cycles. XCT could also be used to analyse powder blends within capsules or DPIs, and could even be utilised as a process-line tool for quality assurance.

All of this current work and future avenues are brought together by the INFORM2020 consortium, a partnership between five UK universities, pharmaceutical companies and technology specialists to improve our understanding of drug deposition performance from molecular scales up to inhaler manufacture. The information provided by XCT is complementary to many of the work packages, from synthonic modelling of carrier and DPI crystals to simulations of the aerosolisation process within an inhaler. Together, these will help develop the next generation of inhaled therapy products.

5. Conclusion

Given how central powders are to the functionality and performance of DPIs, accurate characterisation of powder micro-structure is of very high value. In this paper, we have demonstrated for the first time how X-ray computed tomography (XCT) can be an analytical characterisation tool for inhaled therapy powders, producing number- and volume-based particle size distributions, shape distributions, and morphological assessment.

We have shown how XCT can inform the powder morphology in a similar fashion to scanning electron microscopy, with lower resolution but with the added value of 3D. Size distributions were comparable between XCT, laser diffraction (LD) and optical microscopy (OM),

[1] https://www.cmac.ac.uk/
[2] https://www.royce.ac.uk/

although XCT were marginally lower due to the fully 3D measurements. Shape distributions were different between XCT and OM, showing the importance of 3D imaging compared to 2D. Proof of concept experiments also showed how XCT can give unique 3D spatial insight into how particle attributes such as size and shape affect the particle arrangements and hence the flowability, with many aspects of microstructure and organisation of the formulations accessible through XCT which are not possible through other methods. Going forwards automated data analysis tools will reduce the skill level and the reproducibility of XCT analyses.

Through this work, we have clearly shown that XCT can be an invaluable, fully 3D and non-destructive powder characterisation technique that has a number of advantages for characterisation of inhalation therapy blends.

CRediT authorship contribution statement

P. Gajjar: Conceptualization, Methodology, Software, Formal analysis, Investigation, Writing - original draft, Writing - review & editing, Visualization. **I.D. Styliari:** Conceptualization, Methodology, Formal analysis, Investigation, Writing - original draft, Writing - review & editing, Visualization. **T.T.H. Nguyen:** Conceptualization, Methodology, Formal analysis, Investigation, Writing - original draft, Writing - review & editing, Visualization. **J. Carr:** Methodology, Software, Writing - review & editing. **X. Chen:** Methodology, Software, Formal analysis, Investigation, Writing - review & editing, Visualization. **J.A. Elliott:** Resources, Writing - review & editing, Supervision, Funding acquisition. **R.B. Hammond:** Resources, Writing - review & editing, Supervision, Funding acquisition. **T.L. Burnett:** Conceptualization, Resources, Writing - review & editing, Supervision, Funding acquisition. **K. Roberts:** Conceptualization, Resources, Writing - review & editing, Supervision, Funding acquisition. **P.J. Withers:** Conceptualization, Resources, Writing - review & editing, Supervision, Funding acquisition. **D. Murnane:** Conceptualization, Resources, Writing - review & editing, Supervision, Project administration, Funding acquisition.

Declaration of Competing Interest

The authors declare that they have no known competing financial interests or personal relationships that could have appeared to influence the work reported in this paper.

Acknowledgements

The authors of this paper are all part of the INFORM2020 consortium, which is funded through the EPSRC grant EP/N025075/1. We are grateful to consortium partner DFE Pharma and to Meggle for providing the raw materials. We further acknowledge 3M, Astra Zeneca, Glaxo Smith Kline, Malvern Panalytical and Carl Zeiss Microscopy for their membership and support of the INFORM2020 consortium. We are grateful to Paul Kippax and Jenny Burt of Malvern Panalytical for assistance with running samples on the g3 Morphologi. PG also acknowledges support from EP/M010619/1. Beamtime was kindly provided by the Henry Moseley X-ray Imaging Facility (HMXIF), which was established through EPSRC grants EP/F007906/1, EP/I02249X/1 and EP/F028431/1. HMXIF is a part of the Henry Royce Institute for Advanced Materials, established through EPSRC grants EP/R00661X/1, EP/P025498/1 and EP/P025021/1.

Appendix A. Supplementary material

Supplementary data associated with this article can be found, in the online version, at https://doi.org/10.1016/j.ejpb.2020.02.013.

References

[1] H.M.B. Al-Hashemi, O.S.B. Al-Amoudi, A review on the angle of repose of granular materials, Powder Technol. 330 (2018) 397–417.
[2] M. Alhijjaj, S. Yassin, M. Reading, J.A. Zeitler, P. Belton, S. Qi, Characterization of heterogeneity and spatial distribution of phases in complex solid dispersions by thermal analysis by structural characterization and X-ray micro computed tomography, Pharm. Res. 34 (5) (2017) 971–989.
[3] S. Beucher, F. Meyer, The morphological approach to segmentation: the watershed transformation, in: E.R. Dougherty (Ed.), Mathematical morphology in image processing, Optical Engineering, Marcel Dekker Inc, Ch. 12, 1993, pp. 433–481.
[4] T.L. Burnett, N.J.H. Holroyd, J.J. Lewandowski, M. Ogurreck, C. Rau, R. Kelley, E.J. Pickering, M. Daly, A.H. Sherry, S. Pawar, T.J.A. Slater, P.J. Withers, Degradation of metallic materials studied by correlative tomography, IOP Conf. Ser.-Mater. Sci. Eng. 219 (1) (2017) 12001.
[5] G. Calvert, M. Ghadiri, M. Dyson, P. Kippax, F. McNeil-Watson, The flowability and aerodynamic dispersion of cohesive powders, Powder Technol. 240 (Supplement C) (2013) 88–94.
[6] M. Capece, K.R. Silva, D. Sunkara, J. Strong, P. Gao, On the relationship of inter-particle cohesiveness and bulk powder behavior: flowability of pharmaceutical powders, Int. J. Pharm. 511 (1) (2016) 178–189.
[7] X. Chen, A comparison of eulerian-eulerian and Eulerian-Lagrangian approaches for modelling the aerosolisation of fine powders, Future Formul. 3 (2019), https://www.formulation.org.uk/ff3-abstracts.html#Chen.
[8] A.R. Clark, Medical aerosol inhalers: past, present, and future, Aerosol Sci. Technol. 22 (4) (1995) 374–391.
[9] C. Darquenne, Particle deposition in the lung, Encyclopedia Respirat. Med. (2006) 300–304.
[10] A.H. de Boer, P. Hagedoorn, M. Hoppentocht, F. Buttini, F. Grasmeijer, H.W. Frijlink, Dry powder inhalation: past, present and future, Expert Opin. Drug Delivery 14 (4) (2017) 499–512 pMID: 27534768.
[11] D. El-Sabawi, S. Edge, R. Price, P.M. Young, Continued investigation into the influence of loaded dose on the performance of dry powder inhalers: surface smoothing effects, Drug Dev. Ind. Pharm. 32 (10) (2006) 1135–1138.
[12] L. Fang, X. Yin, L. Wu, Y. He, Y. He, W. Qin, F. Meng, P. York, X. Xu, J. Zhang, Classification of microcrystalline celluloses via structures of individual particles measured by synchrotron radiation X-ray micro-computed tomography, Int. J. Pharm. 531 (2) (2017) 658–667.
[13] J.C. Feeley, P. York, B.S. Sumby, H. Dicks, Determination of surface properties and flow characteristics of salbutamol sulphate, before and after micronisation, Int. J. Pharm. 172 (1–2) (1998) 89–96.
[14] L.A. Feldkamp, L.C. Davis, J.W. Kress, Practical cone-beam algorithm, J. Opt. Soc. Am. A 1 (6) (1984) 612–619.
[15] H.W. Frijlink, A.H. De Boer, Dry powder inhalers for pulmonary drug delivery, Expert Opin. Drug Delivery 1 (1) (2004) 67–86 pMID: 16296721.
[16] X. Fu, M. Dutt, A.C. Bentham, B.C. Hancock, R.E. Cameron, J.A. Elliott, Investigation of particle packing in model pharmaceutical powders using X-ray microtomography and discrete element method, Powder Technol. 167 (3) (2006) 134–140.
[17] P. Gajjar, J.S. Jørgensen, J.R.A. Godinho, C.G. Johnson, A. Ramsey, P.J. Withers, New software protocols for enabling laboratory based temporal CT, Rev. Sci. Instrum. 89 (9) (2018) 93702.
[18] R. Han, G. Papadopoulos, B.J. Greenspan, Investigation of powder dispersion inside a SPIROS® dry powder inhaler using particle image velocimetry, Powder Technol. 125 (2002) 266–278, https://doi.org/10.1016/S0032-5910(01)00515-0.
[19] B.C. Hancock, M.P. Mullarney, X-ray microtomography of solid dosage forms, Pharm. Technol. 29 (4) (2005) 92–100.
[20] M.S. Hassan, R.W.M. Lau, Effect of particle shape on dry particle inhalation: Study of flowability, aerosolization, and deposition properties, AAPS PharmSciTech 10 (4) (2009) 1252.
[21] Y. Hattori, T. Takaku, M. Otsuka, Mechanochemical effect on swelling and drug release of natural polymer matrix tablets by X-ray computed tomography, Int. J. Pharm. 539 (1–2) (2018) 31–38.
[22] A.J. Hickey, H.M. Mansour, M.J. Telko, Z. Xu, H.D.C. Smyth, T. Mulder, R. McLean, J. Langridge, D. Papadopoulos, Physical characterization of component particles included in dry powder inhalers. i. strategy review and static characteristics, J. Pharm. Sci. 96 (5) (2007) 1282–1301.
[23] R. Ho, A.S. Muresan, G.A. Hebbink, J.Y.Y. Heng, Influence of fines on the surface energy heterogeneity of lactose for pulmonary drug delivery, Int. J. Pharm. 388 (1–2) (2010) 88–94.
[24] M. Hoppentocht, P. Hagedoorn, H.W. Frijlink, A.H. de Boer, Technological and practical challenges of dry powder inhalers and formulations, Adv. Drug Deliv. Rev. 75 (2014) 18–31, https://doi.org/10.1016/j.addr.2014.04.004.
[25] S. Jaffari, B. Forbes, E. Collins, D.J. Barlow, G.P. Martin, D. Murnane, Rapid characterisation of the inherent dispersibility of respirable powders using dry dispersion laser diffraction, Int. J. Pharm. 447 (1–2) (2013) 124–131.
[26] M.D. Jones, R. Price, The influence of fine excipient particles on the performance of carrier-based dry powder inhalation formulations, Pharm. Res. 23 (8) (2006) 1665–1674.
[27] W. Kaialy, M. Ticehurst, A. Nokhodchi, Dry powder inhalers: mechanistic evaluation of lactose formulations containing salbutamol sulphate, Int. J. Pharm. 423 (2) (2012) 184–194.
[28] R. Kajihara, S. Noguchi, Y. Iwao, Y. Yasuda, M. Segawa, S. Itai, Structural investigation of spherical hollow excipient Mannit Q by X-ray microtomography, Int. J. Pharm. 495 (1) (2015) 140–143.

[29] J. Kastner, Special issue on the 6th conference on industrial computed tomography 2016 (iCT2016). Case Studies in Nondestructive Testing and Evaluation 6 (B), 2–3, Special Issue: Industrial computed tomography, (2016).
[30] M. Kenward, Advanced materials receives big push to bridge uk university-industry gap: www.royce.ac.uk, MRS Bull. 42 (6) (2017) 410–411.
[31] H. Kinnunen, G. Hebbink, H. Peters, J. Shur, R. Price, An Investigation into the effect of fine lactose particles on the fluidization behaviour and aerosolization performance of carrier-based dry powder inhaler formulations, AAPS PharmSciTech 15 (4) (2014) 898–909.
[32] T. Kojima, J.A. Elliott, Incipient flow properties of two-component fine powder systems and their relationships with bulk density and particle contacts, Powder Technol. 228 (2012) 359–370.
[33] T. Kopsch, D. Murnane, D. Symons, Optimizing the entrainment geometry of a dry powder inhaler: methodology and preliminary results, Pharm. Res. 33 (11) (2016) 2668–2679.
[34] X. Kou, L.W. Chan, H. Steckel, P.W.S. Heng, Physico-chemical aspects of lactose for inhalation, Adv. Drug Deliv. Rev. 64 (3) (2012) 220–232.
[35] D.R. Kryscio, P.M. Sathe, R. Lionberger, L. Yu, M.A. Bell, M. Jay, J.Z. Hilt, Spreadability measurements to assess structural equivalence (Q3) of topical formulations – a technical note, AAPS PharmSciTech 9 (1) (2008) 84–86.
[36] V.N.P. Le, E. Robins, M.P. Flament, Agglomerate behaviour of fluticasone propionate within dry powder inhaler formulations, Eur. J. Pharm. Biopharm. 80 (3) (2012) 596–603.
[37] D. Lu, S.L. Lee, R.A. Lionberger, S. Choi, W. Adams, H.N. Caramenico, B.A. Chowdhury, D.P. Conner, R. Katial, S. Limb, J.R. Peters, L. Yu, S. Seymour, B.V. Li, International guidelines for bioequivalence of locally acting orally inhaled drug products: similarities and differences, AAPS J. 17 (3) (2015) 546–557.
[38] E. Maire, P.J. Withers, Quantitative X-ray tomography, Int. Mater. Rev. 59 (1) (2014) 1–43.
[39] D. Markl, A. Strobel, R. Schlossnikl, J. Bøtker, P. Bawuah, C. Ridgway, J. Rantanen, T. Rades, P. Gane, K.-E. Peiponen, J.A. Zeitler, Characterisation of pore structures of pharmaceutical tablets: a review, Int. J. Pharm. 538 (1) (2018) 188–214.
[40] S.C. Mayo, A.W. Stevenson, S.W. Wilkins, In-line phase-contrast X-ray imaging and tomography for materials science, Materials 5 (5) (2012) 937–965.
[41] C. Merusi, G. Brambilla, E.J. Long, G.K. Hargrave, H.K. Versteeg, Optical diagnostics studies of air flow and powder fluidisation in Nexthaler®. Part II: Use of fluorescent imaging to characterise transient release of fines from a dry powder inhaler, Int. J. Pharm. 549 (1–2) (2018) 96–108.
[42] J.D. Miller, C.L. Lin, A.B. Cortes, A review of X-ray computed tomography and its applications in mineral processing, Miner. Process. Extr. Metall. Rev. 7 (1) (1990) 1–18.
[43] M.E. Mullins, L.P. Michaels, V. Menon, B. Locke, M.B. Ranade, Effect of geometry on particle adhesion, Aerosol Sci. Technol. 17 (2) (1992) 105–118.
[44] T.T.H. Nguyen, R.B. Hammond, D. Murnane, K.J. Roberts, A pathway from crystal structure to crystal morphology and crystal surface properties of -lactose monohydrate, linked to powder cohesion and surface interaction forces in agglomerated powders for inhalation drug formulation, 2020 (in preparation).
[45] S. Noguchi, R. Kajihara, Y. Iwao, Y. Fujinami, Y. Suzuki, Y. Terada, K. Uesugi, K. Miura, S. Itai, Investigation of internal structure of fine granules by micro-tomography using synchrotron X-ray radiation, Int. J. Pharm. 445 (1–2) (2013) 93–98.
[46] M. Otsuka, K. Ibe, Y. Tokudome, H. Ohshima, Nano- and macro-geometrical structural change of caffeine and theophylline anhydrate tablets during hydration process by using X-ray computed tomography, Colloids Surf., B 73 (2) (2009) 351–359.
[47] T. Peng, S. Lin, B. Niu, X. Wang, Y. Huang, X. Zhang, G. Li, X. Pan, C. Wu, Influence of physical properties of carrier on the performance of dry powder inhalers, Acta Pharm. Sin. B 6 (4) (2016) 308–318.
[48] G. Perfetti, E.V. de Casteele, B. Rieger, W.J. Wildeboer, G.M. Meesters, X-ray micro tomography and image analysis as complementary methods for morphological characterization and coating thickness measurement of coated particles, Adv. Powder Technol. 21 (2010) 663–675, https://doi.org/10.1016/j.apt.2010.08.002.
[49] G. Pilcer, N. Wauthoz, K. Amighi, Lactose characteristics and the generation of the aerosol, Adv. Drug Deliv. Rev. 64 (3) (2012) 233–256.
[50] R. Price, G. Farias, W. Ganley, J. Shur, Demonstrating Q3 structural equivalence of dry powder inhaler blends: New analytical concepts and techniques, Respirat. Drug Delivery, 2018, pp. 265–276.
[51] S.L. Raghavan, R.I. Ristic, D.B. Sheen, J.N. Sherwood, The bulk crystallization of α-lactose monohydrate from aqueous solution, J. Pharm. Sci. 90 (7) (2001) 823–832.
[52] C. Redenbach, R. Ohser-Wiedemann, R. Löffler, T. Bernthaler, A. Nagel, Characterization of powders using micro computed tomography, Part. Part. Syst. Char. 28 (1–2) (2012) 3–12.
[53] J. Rudén, G. Frenning, T. Bramer, K. Thalberg, G. Alderborn, Relationships between surface coverage ratio and powder mechanics of binary adhesive mixtures for dry powder inhalers, Int. J. Pharm. 541 (1–2) (2018) 143–156.
[54] J. Rudén, G. Frenning, T. Bramer, K. Thalberg, J. An, G. Alderborn, Linking carrier morphology to the powder mechanics of adhesive mixtures for dry powder inhalers via a blend-state model, Int. J. Pharm. 561 (2019) 148–160, https://doi.org/10.1016/j.ijpharm.2019.02.038.
[55] U.V. Shah, V. Karde, C. Ghoroi, J.Y. Heng, Influence of particle properties on powder bulk behaviour and processability, Int. J. Pharm. 518 (1–2) (2017) 138–154.
[56] H. Shi, R. Mohanty, S. Chakravarty, R. Cabiscol, M. Morgeneyer, H. Zetzener, J.Y. Ooi, A. Kwade, S. Luding, V. Magnanimo, Effect of particle size and cohesion on powder yielding and flow, KONA Powder Particle J. 35 (2018) 226–250, https://doi.org/10.14356/kona.2018014 2018014.
[57] J. Shur, R. Price, Advanced microscopy techniques to assess solid-state properties of inhalation medicines, Adv. Drug Deliv. Rev. 64 (4) (2012) 369–382.
[58] P. Singh, P. Ramakrishnan, Powder Characterization by Particle Shape Assessment, Kona Powder Particle J. 14 (1996) 16–30.
[59] I.C. Sinka, S.F. Burch, J.H. Tweed, J.C. Cunningham, Measurement of density variations in tablets using X-ray computed tomography, Int. J. Pharm. 271 (1–2) (2004) 215–224.
[60] J.A. Slotwinski, E.J. Garboczi, P.E. Stutzman, C.F. Ferraris, S.S. Watson, M.A. Peltz, Characterization of metal powders used for additive manufacturing, J. Res. Nat. Inst. Stand. Technol. 119 (2014) 460–493.
[61] N. Stanley-Wood, M. Sarrafi, Z. Mavere, M. Schaefer, The relationships between powder flowability, particle re-arrangement, bulk density and jenike failure function, Adv. Powder Technol. 4 (1) (1993) 33–40.
[62] N. Stevens, J. Shrimpton, M. Palmer, D. Prime, B. Johal, Accuracy assessments for laser diffraction measurements of pharmaceutical lactose, Meas. Sci. Technol. 18 (12) (2007) 3697–3706.
[63] S.R. Stock, X-ray microtomography of materials, Int. Mater. Rev. 44 (4) (1999) 141–164.
[64] M.J. Telko, A.J. Hickey, Dry powder inhaler formulation, Respirat. Care 50 (9) (2005) 1209–1227.
[65] K. Thalberg, D. Lindholm, A. Axelsson, Comparison of different flowability tests for powders for inhalation, Powder Technol. 146 (3) (2004) 206–213.
[66] R. Tuley, J. Shrimpton, M.D. Jones, R. Price, M. Palmer, D. Prime, Experimental observations of dry powder inhaler dose fluidisation, Int. J. Pharm. 358 (1–2) (2008) 238–247.
[67] T.D. Turner, P. Gajjar, I. Fragkopoulos, J. Carr, T.T.H. Nguyen, D. Hooper, F. Clarke, N. Dawson, P.J. Withers, K.J. Roberts, Measuring particle packing of glutamic acid through X-ray computed tomography for understanding powder flow and consolidation behaviour, Cryst. Growth Des. (2020) (submitted for publication).
[68] A. Videla, C.-L. Lin, J.D. Miller, Watershed functions applied to a 3D image segmentation problem for the analysis of packed particle beds, Particle Particle Syst. Char. 23 (3–4) (2006) 237–245.
[69] S. Weis, M. Schröter, Analyzing X-ray tomographies of granular packings, Rev. Sci. Instrum. 88 (5) (2017) 51809.